

# PROCEEDINGS OF SPIE

[SPIEDigitalLibrary.org/conference-proceedings-of-spie](https://SPIEDigitalLibrary.org/conference-proceedings-of-spie)

## Nanoscale inhomogeneity and photoacid generation dynamics in extreme ultraviolet resist materials

Wu, Ping-Jui, Wang, Yu-Fu, Chen, Wei-Chi, Wang, Chien-Wei, Cheng, Joy, et al.

Ping-Jui Wu, Yu-Fu Wang, Wei-Chi Chen, Chien-Wei Wang, Joy Cheng, Vencent Chang, Ching-Yu Chang, John Lin, Yuan-Chung Cheng, "Nanoscale inhomogeneity and photoacid generation dynamics in extreme ultraviolet resist materials," Proc. SPIE 10586, Advances in Patterning Materials and Processes XXXV, 105861O (13 March 2018); doi: 10.1117/12.2316308

**SPIE.**

Event: SPIE Advanced Lithography, 2018, San Jose, California, United States

# Nanoscale inhomogeneity and photoacid generation dynamics in extreme ultraviolet resist materials

Ping-Jui Wu<sup>1</sup>, Yu-Fu Wang<sup>1</sup>, Wei-Chi Chen<sup>1</sup>, Chien-Wei Wang<sup>2</sup>, Joy Cheng<sup>2</sup>, Vencent Chang<sup>2</sup>, Ching-Yu Chang<sup>2</sup>, John Lin<sup>2</sup>, Yuan-Chung Cheng<sup>1</sup>

<sup>1</sup>Department of Chemistry and Center for Quantum Science and Engineering, National Taiwan University, Taipei 106, Taiwan

<sup>2</sup>nPtD, Taiwan Semiconductor Manufacturing Company, Ltd., Hsinchu 300, Taiwan

## ABSTRACT

The development of extreme ultraviolet (EUV) lithography towards the 22 nm node and beyond depends critically on the availability of resist materials that meet stringent control requirements in resolution, line edge roughness, and sensitivity. However, the molecular mechanisms that govern the structure-function relationships in current EUV resist systems are not well understood. In particular, the nanoscale structures of the polymer base and the distributions of photoacid generators (PAGs) should play a critical roles in the performance of a resist system, yet currently available models for photochemical reactions in EUV resist systems are exclusively based on homogeneous bulk models that ignore molecular-level details of solid resist films. In this work, we investigate how microscopic molecular organizations in EUV resist affect photoacid generations in a bottom-up approach that describes structure-dependent electron-transfer dynamics in a solid film model. To this end, molecular dynamics simulations and stimulated annealing are used to obtain structures of a large simulation box containing poly(4-hydroxystyrene) (PHS) base polymers and triphenylsulfonium based PAGs. Our calculations reveal that ion-pair interactions govern the microscopic distributions of the polymer base and PAG molecules, resulting in a highly inhomogeneous system with nonuniform nanoscale chemical domains. Furthermore, the theoretical structures were used in combination of quantum chemical calculations and the Marcus theory to evaluate electron transfer rates between molecular sites, and then kinetic Monte Carlo simulations were carried out to model electron transfer dynamics with molecular structure details taken into consideration. As a result, the portion of thermalized electrons that are absorbed by the PAGs and the nanoscale spatial distribution of generated acids can be estimated. Our data reveal that the nanoscale inhomogeneous distributions of base polymers and PAGs strongly affect the electron transfer and the performance of the resist system. The implications to the performances of EUV resists and key engineering requirements for improved resist systems will also be discussed in this work. Our results shed light on the fundamental structure dependence of photoacid generation and the control of the nanoscale structures as well as base polymer-PAG interactions in EUV resist systems, and we expect these knowledge will be useful for the future development of improved EUV resist systems.

## 1. INTRODUCTION

In extreme ultraviolet (EUV) lithography, 13.5 nm light is used to induce photoacid generation that consequently leads to dissolution of polymers. The resist chemistry in EUV exposure is markedly different from that in photolithography utilizing 193- or 248-nm photons.<sup>1,2</sup> Specifically, the absorption of high energy EUV light leads to electron dissociation and generation of multiple electrons, and these electrons then rapidly thermalized and react with photoacid generators (PAGs) to induce acid production. Indeed, the secondary electrons generated by ionization of the polymer backbone is considered to play a key role in the acid generation.<sup>3,4</sup> As a result, diffusion of thermalized electrons plays a critical role in the control of resolution, line edge roughness, and sensitivity in EUV lithography.

Despite the early recognition of the importance of electron dynamics in EUV lithography, both theoretical and experimental mechanistic studies of EUV resist chemistry often focus on the dynamics of acid diffusion and quenching. It is challenging to develop tools that are specifically sensitive to electronic responses in resist

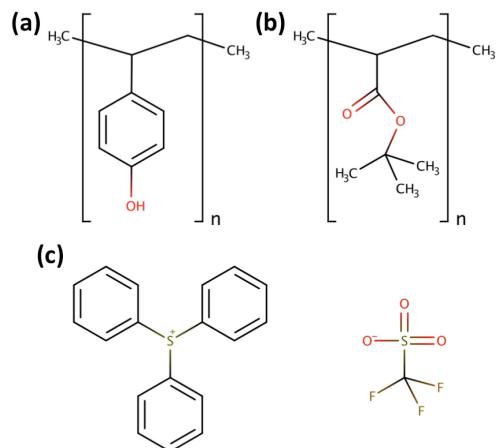


Figure 1. Chemical structures of the components in the model systems. (a) a poly(4-hydroxystyrene) (PHS) unit, (b) a *tert*-butyl acrylate (TBA) unit, and (c) the TPS-TfI salt.

matrix for effective probe of electron dynamics. Recently, Brainard and coworkers have developed a low-energy electron scattering in solids modeling program that tracks elastic, ionization, and plasmon generation events for high-energy electrons in resist matrix to investigate detailed electron dynamics in EUV lithography, and their results have suggested novel resist design principles by supporting a new mechanism for acid generation in the process.<sup>4,5</sup> Clearly, a clear understanding of electron dynamics in EUV lithography is extremely critical for the optimization of the process.

A key issue that was mostly overlooked in previous studies of EUV resist chemistry is the heterogeneity of the resist matrix. The theoretical modeling of electron propagation in previous studies always assume an uniform bulk matrix.<sup>1</sup> However, the resist is composed of several components that might not mix very well in the nanometer length scale. Recently, molecular dynamics simulations have been applied to investigate PAG distributions in a methacrylate-type model resist system.<sup>6,7</sup> The results show significant nanoscale heterogeneity that could affect resist properties such as resolution, line edge roughness, and sensitivity. It is expected that this issue would become more critical as the required line width shrinks to below 10 nm. In this work, we utilize molecular dynamics simulations and stimulated annealing to obtain structures of a simulation box containing poly(4-hydroxystyrene) (PHS) base polymers and triphenylsulfonium (TPS) based PAGs to investigate how microscopic molecular organizations in EUV resist could affect photoacid generations in EUV lithography. Furthermore, the obtained atomistic structure will then be used to simulate structure-dependent electron-transfer dynamics in a solid film model. We expect such bottom-up approach could provide rich molecular insights regarding the heterogeneous domain distributions and electron transfer dynamics in EUV resist materials, which is critical for advancing the technology of EUV resist lithography.

## 2. COMPUTATIONAL METHODS

### 2.1 Molecular dynamics simulations

In this study, we investigate resist systems based on PHS and *tert*-butyl acrylate (TBA) copolymers and a TPS-triflate PAG (Fig. 1). Two polymer systems were constructed in this study: one is a PHS-rich model that contains copolymers of 10 units of PHS, 10 units of TBA, and 10 units of PHS in each chain, the other one is a TBA-rich model that contains copolymers of 10 units of TBA, 10 units of PHS, and 10 units of TBA in each chain. The selection of the model systems aims to elucidate the effects of a PHS-rich matrix versus a TBA-rich matrix. An extreme block-copolymer form is also adopted in this study in order to maximize the difference if observed in the simulated results, and the total chain length of 30 units is chosen to reflect the molecular weights of copolymers normally used in experiments. Matrix with copolymers with randomly arranged PHS and TBA units would be a better representation of the realistic resist systems, however in that case the comparison might be more difficult to yield useful guiding principles.

Amorphous resist models were built with 64 copolymer chains and 128 TPS-Tf ion pairs in a simulation box, which represents about 20% wt. PAG density. For both types of resist matrices, the simulation box contains > 40000 atoms. Periodic boundary condition is used in all our simulations, and the MM3 force field suitable for crystal packing and thermodynamics data for organic molecules is adopted for our molecular dynamics simulations.<sup>8-10</sup> In order to examine the structures of co-polymer systems, we have simulated the equilibrium structures of the chemical units used in this study (Fig. 1) using the MM3 force field and confirm that the geometries are in good agreement with those calculated using *ab initio* density functional theory (DFT) at the B3LYP/6-31+G\* level.

The TINKER molecular modeling software<sup>11</sup> with the OpenMP parallelization is used to carry out molecular dynamics simulations of the resist model systems. The initial geometries of the randomized amorphous resist models were optimized using the steepest descent and conjugated gradient methods, and then subjected to 5 cycles of 10 ps run simulated annealing between 300K and 1000K within the NPT ensemble at 1 atm. The Berendsen thermostat<sup>12</sup> was used for both pressure and temperature controls. After simulated annealing, the simulation box is compressed to reach a desired density of ~1 g/cm<sup>3</sup>, and the geometry is used as the initial input for the equilibrium run. The equilibrium step is then performed with NPT molecular dynamics simulation at 300K and 1 atm for 100 ps. We monitor the energy and density fluctuations to ensure that the steady state is reached in the final 30 ps frame. Finally, production run is carried out at 300K and 1 atm for 5 ns. A total of 5000 snapshots of the molecular dynamics trajectory are collected at 1 ps interval as the results. The same procedures were used for both PHS-rich and TBA-rich matrices.

## 2.2 Electron transfer rates

With the structures obtained from the molecular dynamics simulations, we could then simulate photo-induced reactions in the resist matrix in a fully atomistic level. Recent studies have shown that several mechanisms, such as hole-initiated chemistry, electron trapping, internal excitation, could be involved in acid production in EUV resist chemistry.<sup>4,5</sup> Different mechanisms of acid productions will lead to different conditions in simulations, nevertheless, transfer of thermalized electrons in the polymer matrix is a key step shared by all the proposed mechanisms. As a result, we aim to focus on the nanoscale structures of the polymer matrix and the consequent effects on the electron transfer events. To simplify the photo-induced dynamics, we adopt the electron trapping mechanism of acid generation, and therefore we shall simulate electron transfer dynamics and calculate the amount of electrons reaching the PAG sites. Therefore, we consider all PhOH molecules and TPS molecules as potential sites that each can harbor an excess electron. Moreover, for each PhOH site, having a hole is also possible. To this end, we need to calculate electron transfer rates between PhOH units and between PhOH and TPS molecules based on the structures obtained from the molecular dynamics simulations.

We follow the quantum chemical parameterization of electron transfer rates that were very success in modeling electron and hole transport in organic photovoltaic materials.<sup>13-17</sup> The electron transfer rate can be calculated using the Marcus theory

$$k_{ET} = \frac{2\pi}{\hbar} |V_{DA}|^2 \frac{1}{\sqrt{4\pi\lambda k_B T}} \exp \left[ \frac{-(\Delta G + \lambda)^2}{4\lambda k_B T} \right],$$

where  $V_{DA}$  is the electron coupling between the electron donor and acceptor,  $\lambda$  is the reorganization energy, and  $\Delta G$  is the free-energy difference. The electron couplings between PhOHs and between PhOHs and TPS molecules were calculated using the Q-Chem quantum chemistry software package by the direct method and the B3LYP/6-31+G\* density functional theory.<sup>18,19</sup> In addition,  $\lambda$  and  $\Delta G$  are also calculated at the B3LYP/6-31+G\* level of theory based on the procedures outlined by Cornil *et al.*<sup>14</sup> Note that in the resist matrix we consider the TPS molecule as a pure electron acceptor, and the PhOH can be in one of the anionic, neutral, and cationic states. The anionic PhOH is an electron donor, the cationic PhOH is a hole donor and electron acceptor (resulting in electron-hole recombination), whereas the neutral PhOH is either an electron acceptor or a hole acceptor. Because all these PhOH states have different electron energies that can be estimated from their molecular orbital energies, we can calculate separate rates for electron transfer, hole transfer, and electron-hole recombination processes. As a result, we can construct a rate matrix connecting all pairs of potential electron donors and acceptors using structure-based quantum chemistry calculations.

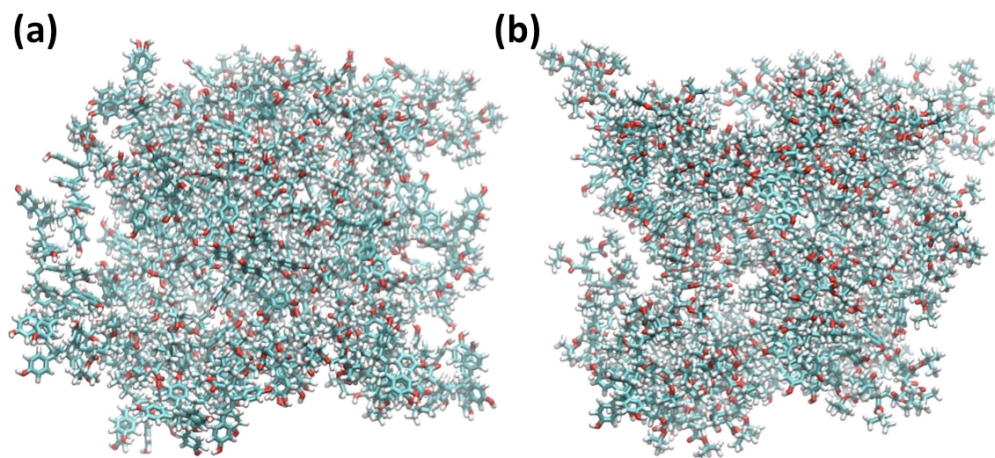


Figure 2. Simulation box of the (a) PhOH-rich matrix and the (b) TBA-rich matrix. Each box contains 64 copolymer chains and 128 TPS-TfI PAG ion pairs. Periodic boundary condition is used in the simulations.

Because the electronic couplings between a donor molecule and an acceptor molecule depend on the relative distance and molecular orientations, the rates are structure-dependent. In addition, electrons on different chemical species exhibit different free energy, leading to different rates for electron transfer, hole transfer, and charge recombination. In general, for neighboring molecules the rates follow the trend we observed: electron transfer from PhOH to TPS > electron transfer from PhOH to PhOH > hole transfer from PhOH to PhOH >> charge recombination on two PhOH sites.

### 2.3 Kinetic Monte Carlo simulations

Using the prescription outlined above, we may construct a rate matrix for a given structure of the resist matrix. The rate matrix is then used in a standard kinetic Monte Carlo method<sup>13,17,20,21</sup> implemented in an in-house code to simulate electron dynamics in the resist matrix. For simplicity, in this work we neglect the EUV absorption and electron cascading processes and simulate the dynamics of a number of thermalized electrons and holes distributed around the center of the simulation box. Therefore, we assume independent thermalized electron and hole distributions, and weak electron-hole Coulomb interactions due to dielectric screening. For the location of electron and holes, our models consider rigid polymer structures and localized electrons and holes on PhOH molecules. Our Monte Carlo simulations describe electron and hole diffusion, electron-hole recombination, and electron transfer to TPS. Note that quenching of electron by electron quenchers is not considered in this study.

## 3. RESULTS AND DISCUSSIONS

### 3.1 Structure of polymer matrix

Representative equilibrium structures of the model resist systems are shown in Fig. 2. The size of the box after stimulated annealing is about  $8 \times 8 \times 8 \text{ nm}^3$ . Molecular dynamics simulations clearly show highly disordered polymer matrix and PAG distributions. An inspection of the 5 ns trajectory indicates low mobilities for all the components, including the smaller PAG ions. Our simulations using significantly larger simulation cell confirm the semi-quantitative observations reported in previous molecular dynamics simulations.<sup>6,7</sup>

To assist the visualization of the heterogeneous structures in the simulated polymer EUV resist models, we depict different components in the simulation box using different colors in the representative structures shown in Fig. 3. Separated domains of phenol (PhOH) groups and TBA groups can be clearly observed in the equilibrium structures, and the nonuniform distribution of PAG molecules is also evident. PhOH domain sizes of  $\sim 2 \text{ nm}$  and  $\sim 1 \text{ nm}$  for the PhOH-rich and TBA-rich polymers, respectively, were determined using a k-mean clustering algorithm based on distance between the centers of phenyl rings. The radius of gyration of the co-polymer chains is determined to be about 1 nm for both copolymer systems. It is interesting to note that the PhOH domain

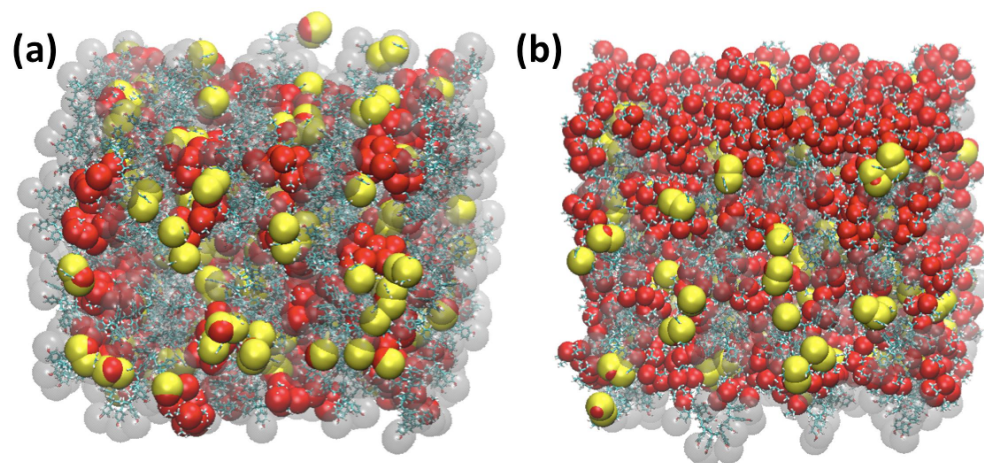


Figure 3. Domain separation in the (a) PhOH-rich matrix and (b) TBA-rich matrix. TBA groups are depicted as red spheres, TPS-Tf molecules are shown in yellow, and the PhOH groups are shown as semi-transparent spheres.

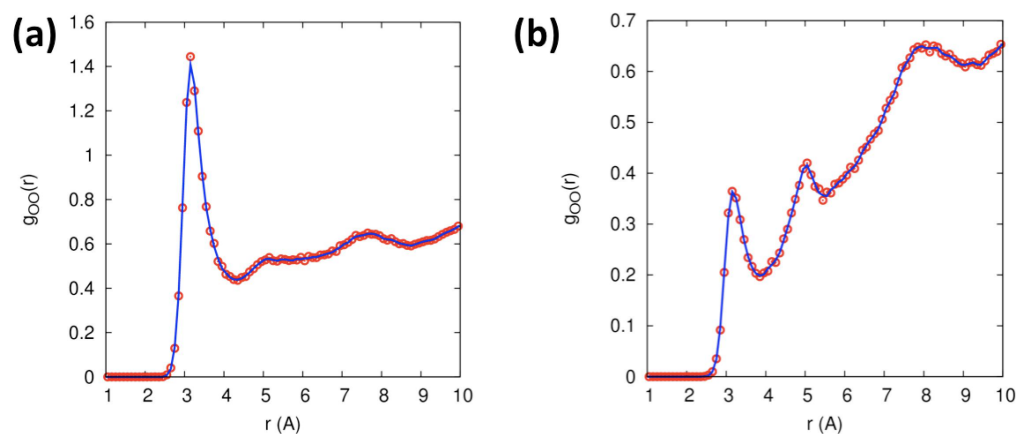


Figure 4. Radial distribution function between phenoxy oxygens in the (a) PhOH-rich matrix and the (b) TBA-rich matrix.

size is noticeably larger than the radius of gyration for the PhOH-rich copolymer chains. This indicates that the intermolecular interactions between PHS groups on different chains play an important role in the nanoscale heterogeneous aggregations of PhOH groups in the polymer matrix.

To quantitatively determine the structural characteristics of the model resist matrix systems, 5000 structure snapshots sampled from the 5 ns trajectory were used to calculate various radial distribution functions for each copolymer system. In Fig. 4, we show radial distribution function between phenoxy oxygens in the PhOH-rich and TBA-rich polymer systems. This radial distribution function characterizes the distance distribution between two PhOH groups. Figure 4(a) shows that the PhOH-rich polymer matrix exhibits a clear structure with a close contact between PhOH groups in about 3 Å, however, the PhOH peak at 3 Å in the TBA-rich matrix is relatively weak (Fig. 4(b)). The radial distribution functions confirm that the PhOH-rich matrix leads to strongly aggregated PhOH domains, whereas the PhOH domain structure in the TBA-rich matrix is disrupted.

Regarding the distribution of the PAGs, we first show the radial distribution functions between TPS and triflate sulfur atoms in Fig. 5. The dominating peak structure at about 3.5 Å is the result of the extremely strong Coulomb attraction between the TPS cation and the triflate anion. Therefore, TPS-triflate ion-pair interactions dominate the distributions of PAGs, in agreement with the observations reported in previous molecular dynamics simulations.<sup>6,7</sup>

More details of the PAG distribution can be determined from inspecting the arrangements of PAG molecules

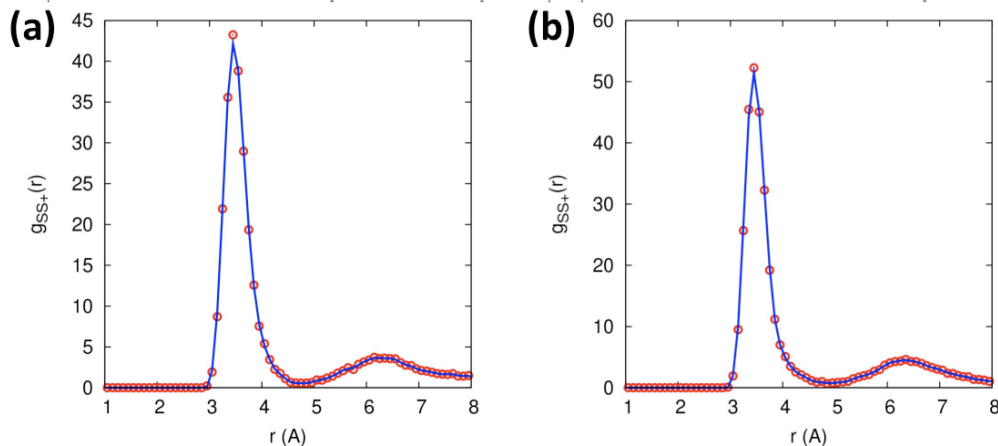


Figure 5. Radial distribution function between TPS and triflate sulfur atoms in the (a) PhOH-rich matrix and the (b) TBA-rich matrix.

relative to either PhOH groups or TBA groups. The radial distribution functions between TPS sulfur atom and TBA carbonyl oxygen shown clear peaked structures ( Figs. 6(a) and 6(b)), which indicate that the TPS cations exhibit strong interactions with the carbonyl group. In contrast, the radial distribution functions between TPS sulfur atom and PhOH phenoxyl oxygen do not exhibit any structure ( Figs. 6(c) and 6(d)), which shows that the TPS cations do not interact specifically with the PhOH group. Moreover, the gradual change in the radial distribution functions in Figs. 6(c) 6(d) suggests that the TPS cations do not mix very well with the PhOH aggregated domain, and most likely TPS cations tend to stay in the TBA domains. We suspect this is due to the size effect of the TPS molecule and the relatively hydrophobic contacts between phenyl rings in the PhOH domain.

Next, we inspect the distribution of triflate ions in the matrix using the radial distribution functions between triflate sulfur atom and TBA carbonyl oxygens (Figs. 7(a) and 7(b)) and that between triflate sulfur atom and PhOH phenoxyl oxygen (Figs. 7(c) and 7(d)). Generally speaking, the triflate anions do not show strong interactions with the TBA group, and only exhibit weak interactions with the PhOH groups. In particular, the triflate anions show a weak tendency to interact with PhOH phenoxyl oxygens at a distance of about 4 Å, which is consistent with a triflate anion interacting with the phenol -OH group through a hydrogen bond. Therefore, electrostatic interactions between phenol protons and anionic triflate ions play a role in controlling the distribution of anions around the PhOH groups.

Interestingly, Figures. 6 and 7 indicate that the TPS cations interact preferentially with the TBA domain, while the triflate anions interact preferentially with the PhOH domain. Considering the dominant ion-pair interactions between the TPS and triflate, this observation logically leads to the conclusion that the PAG ion pairs should preferentially arrange at the boundary between the PhOH domain and TBA domain. To confirm this phenomenon, we show the distributions of molecular components in a 2-nm slice of the simulation box in Fig. 8. The cross section clearly shows nanoscale domains in the matrix and distribution of PAG molecules between the domains. Furthermore, we note that since TPS do not interact strongly with PhOH, the relative position of TPS to PhOH groups (i.e. preferred electron donors) is controlled by how the anions drag TPS cations towards the PhOH domain. This observation offers an explanation of the counter ion effects in EUV resist properties.

### 3.2 Electron transfer dynamics

Kinetic Monte Carlo simulations were carried out based on the electron transfer rates determined from equilibrium positions of PhOH groups and TPS molecules to model electron transfer dynamics with molecular structure details taken into consideration. For simplicity, we ignore the electron cascading dynamics and focus on the diffusion of thermalized electrons in the polymer matrix by considering an initial Gaussian distribution of electrons and holes both with  $\sigma = 1$  nm at the center of the box, and then use kinetic Monte Carlo to follow the consequent electron diffusion, electron-hole recombination, and electron trapping by TPS (TPS activation) events.

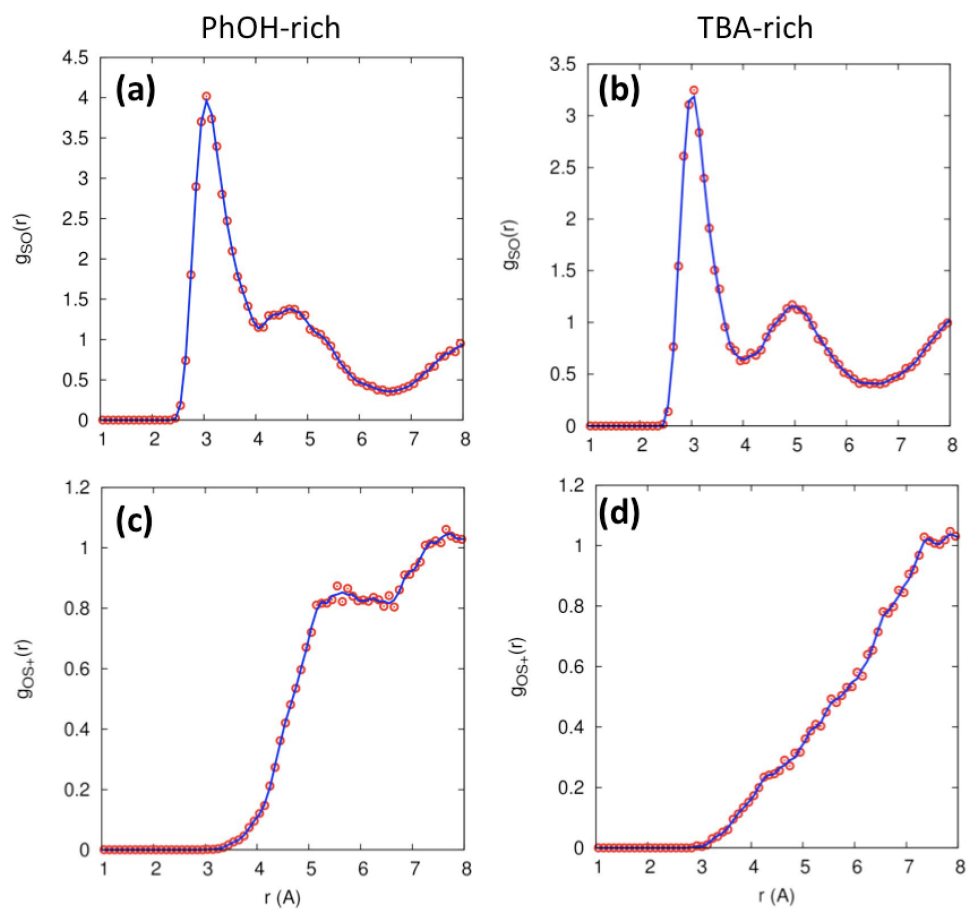


Figure 6. Distribution of TPS in the matrix. We show radial distribution functions between TPS sulfur atom and (a) TBA cabonyl oxygen in the PhOH-rich matrix, (b) TBA cabonyl oxygen in the TBA-rich matrix, (c) PhOH phenoxyl oxygen in the PhOH-rich matrix, and (d) PhOH phenoxyl oxygen in the TBA-rich matrix.

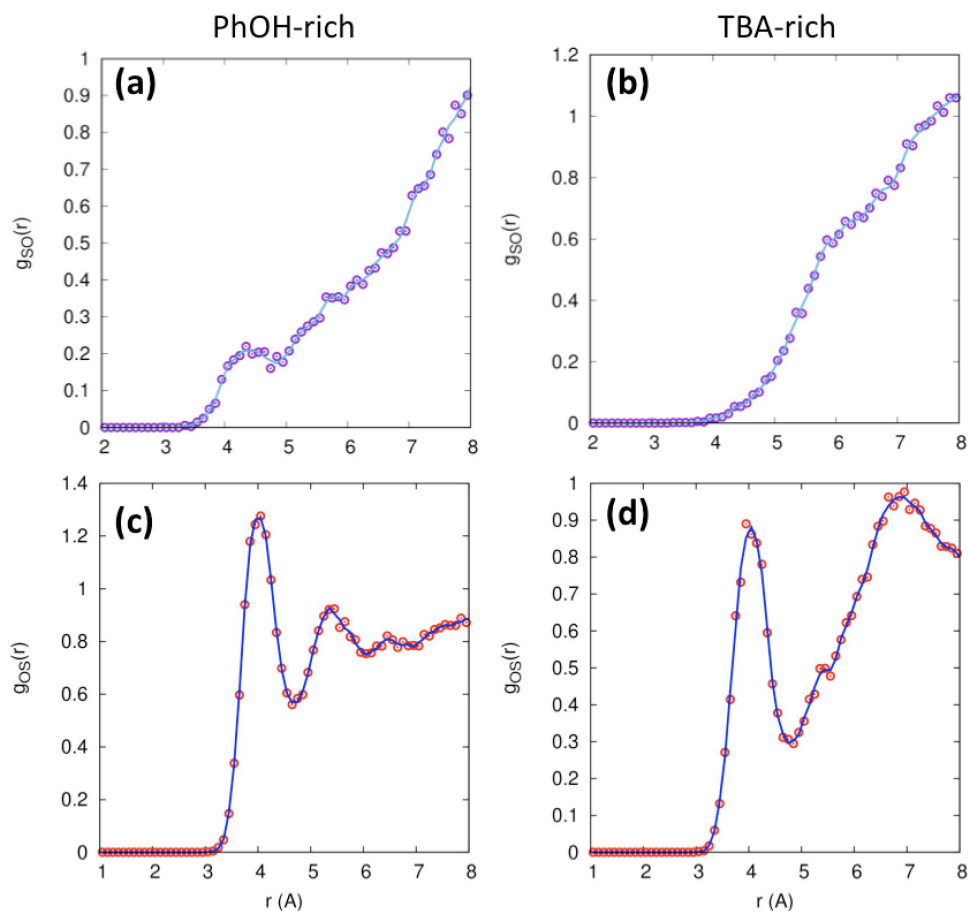


Figure 7. Distribution of triflate ions in the matrix. We show radial distribution functions between triflate sulfur atom and (a) TBA carbonyl oxygen in the PhOH-rich matrix, (b) TBA carbonyl oxygen in the TBA-rich matrix, (c) PhOH phenoxyl oxygen in the PhOH-rich matrix, and (d) PhOH phenoxyl oxygen in the TBA-rich matrix.

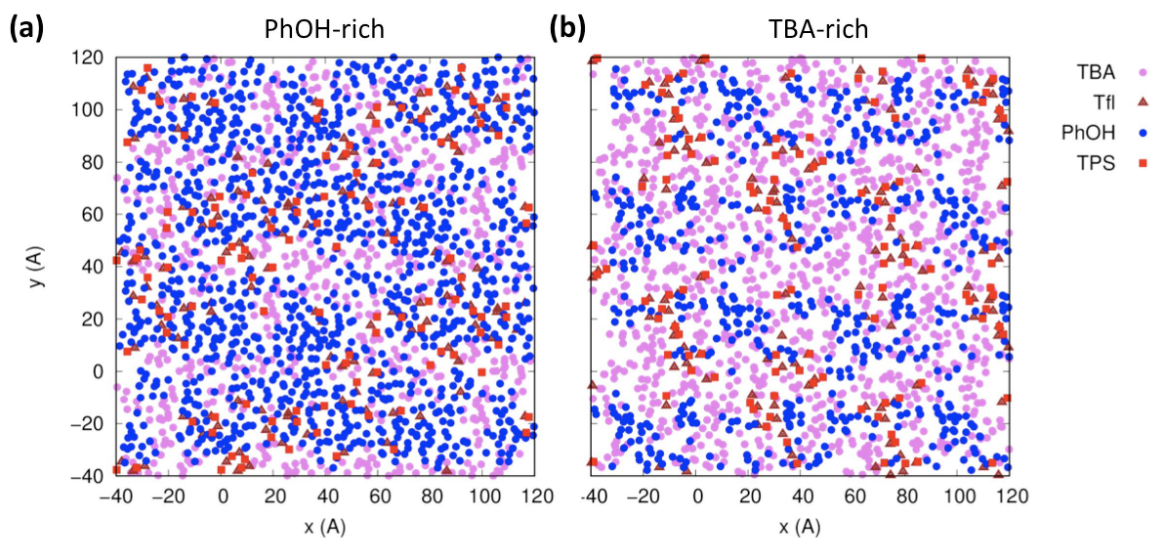


Figure 8. Distribution of molecular moieties in a 2-nm slice of the model resist matrix in the (a) PhOH-rich matrix and (b) TBA-rich matrix.

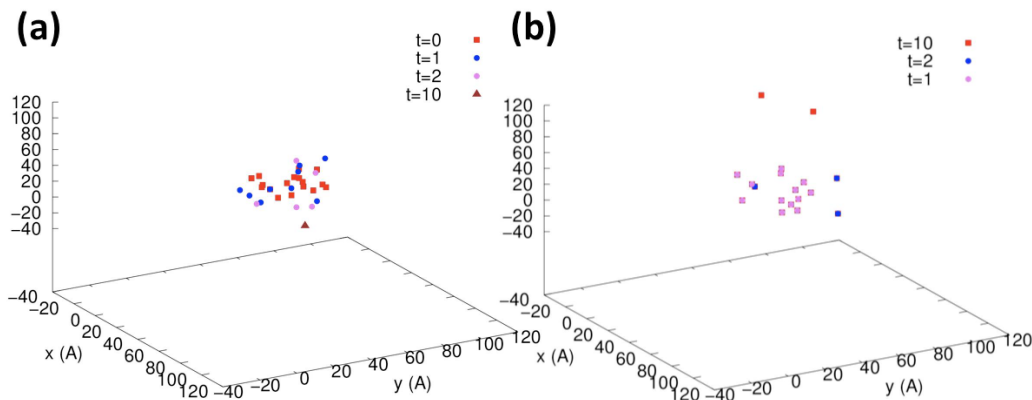


Figure 9. Electron diffusion in the model PhOH-rich matrix using a low excitation density initial condition. We show (a) time-dependent distribution of electrons and (b) distribution of activated PAGs.

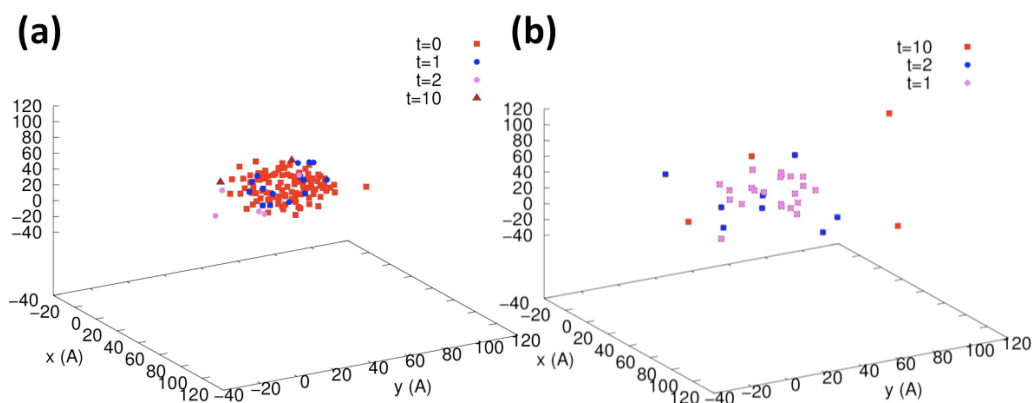


Figure 10. Electron diffusion in the model PhOH-rich matrix using a high excitation density initial condition. We show (a) time-dependent distribution of electrons and (b) distribution of activated PAGs.

A realization of the stochastic trajectory of electron distributions under a low-excitation intensity initial condition (i.e. number of initial electrons less than 20% of the phenol groups in the excitation volume) is shown in Fig. 9(a). There, the diffusion of electrons can be seen in the spreading of the electro distribution, and the reduction of the number of electrons represents the electron loss through electron-hole recombination and electron trapping by TPS. In Fig. 9(b), the distribution of activated TPS sites is shown as a function of time. In this case most electrons are successfully trapped by TPS (ratio of the number of electrons reaching TPS over the number of total initial electrons  $> 90\%$ ), which is attributable to the significantly lower electron-hole recombination rate in comparison to the electron transfer and TPS trapping rates.

We have also simulated the electron dynamics at higher initial electron densities (Fig. 10). In this case, initial electron density and hole density are both high, therefore the initial electron dynamics are dominated by electron-hole recombination. As a result, the quantum yield of TPS activation (the number of electrons reaching TPS over the number of total initial electrons) decreases as the initial electron intensity increases. Higher excitation intensity does not generate more activated TPS molecules. Our simulations suggest that quantum yield of PAG activation in EUV resist materials could exhibit highly nonlinear dependence on excitation intensity due to electron-hole recombination processes. Note that here we do not make direct connection between the thermalized electron density and the EUV light intensity, since the absorption and electron cascading processes are not considered in this preliminary study. A quantitative investigation that incorporate more realistic excitation conditions and additional electron dynamical channels is currently a work in progress.

## 4. CONCLUSIONS

We have applied a combination of molecular dynamics simulations and kinetic Monte Carlo modeling to provide structural and electron transfer properties of model resist systems in EUV lithography. Simulations of HOS<sub>2</sub>STyr-TBA copolymers with TPS-triflate additives (~20% wt.) have been carried out for a PHS-rich and a TBS-rich resist models, respectively. We show that the copolymer matrix exhibits segregations of nanoscale PHS and TBA domains, and the PAG distributions are also highly heterogeneous in the nanometer length scale. More detailed analysis indicates that the ion-pair interactions dominate the distributions of PAG molecules. Furthermore, the TPS cations interact preferentially with the TBA domain, while the triflate anions interact preferentially with the PhOH domain, resulting in a preferential distribution of PAG molecules at the interfaces of the PHS and TBA domains. Our model indicates that the relative position of TPS to PhOH groups is controlled by how the anions drag TPS cations towards the PhOH domain, which offers an explanation of the counter ion effects in EUV resist properties. Finally, we study density inhomogeneity in HOS<sub>2</sub>STyr-TBA-TPSTfI copolymer systems, and strong inhomogeneity in the 1 nm length scale can be determined.

The simulated equilibrium geometries of the PhOH-rich resist model were utilized to estimate electron transfer rates by using quantum chemical calculations. We then use these rates to simulate diffusion of thermalized electrons in 16-nm box to yield distributions of electrons and activated PAGs (TPS). Electron dynamics dependence on electron density was studied to show highly nonlinear behavior due to electron-hole recombinations at high initial electron densities, which suggests that quantum yield of electron transfer to PAG in EUV resist materials could depend on excitation intensity. Furthermore, anomalous diffusions of electrons along the polymer longitudinal direction were observed, which could significantly change the electron (acid) profile in the resist matrix. As a result, limiting electron transfer along the polymer chain might be an effective method to stop unintended long-range electron transfer events.

In summary, our preliminary results indicate that molecular dynamics simulations and quantum chemistry calculations could be combined to provide molecular-level simulations of electronic dynamics in EUV resist systems, and the nanoscale heterogeneity could critically affect the developments of patterns in EUV lithography. The theoretical framework demonstrated in this work could be combined with models for electron generation/cascading<sup>1,5</sup> and acid production/diffusion to enable a molecular-level understanding of EUV photo-induced physics and chemistry in various resist systems. Such bottom-up elucidation of structure-function relationships for resist systems could play important roles in the advancement of EUV resist lithography.

## REFERENCES

1. Takahiro Kozawa and Seiichi Tagawa. Radiation Chemistry in Chemically Amplified Resists. *Jpn. J. Appl. Phys.*, 49, 2010.
2. Toshiro Itani. A Comprehensive Review of EUV Resist Materials and Processing at Selete. *J. Photopolym. Sci. Tec.*, 24:111–118, 2011.
3. Hiroki Yamamoto, Takahiro Kozawa, Seiichi Tagawa, Heidi B Cao, Hai Deng, and Michael J Leeson. Polymer-structure dependence of acid generation in chemically amplified extreme ultraviolet resists. *Jpn. J. Appl. Phys.*, 46:L142–L144, 2007.
4. Justin Torok, Ryan Del Re, Henry Herbol, Sanjana Das, Irina Bocharova, Angela Paolucci, Leonidas E Ocola, Carl Jr Ventrice, Eric Lifshin, Greg Denbeaux, and Robert L Brainard. Secondary Electrons in EUV Lithography. *J. Photopolym. Sci. Tec.*, 26:625–634, 2013.
5. Amrit Narasimhan, Steven Grzeskowiak, Christian Ackerman, Tracy Flynn, Greg Denbeaux, and Robert Brainard. Mechanisms of euv exposure: electrons and holes, 2017.
6. Minoru Toriumi and Toshiro Itani. Inhomogeneity of PAGs in Resist Film studied by Molecular Dynamics Simulations. *J. Photopolym. Sci. Tec.*, 27:617–622, 2014.
7. Minoru Toriumi and Toshiro Itani. Inhomogeneity of photoacid generators in methacrylate-type EUV resist film studied by molecular dynamics simulations. *Jpn. J. Appl. Phys.*, 54:06FE02, 2015.
8. Norman L. Allinger, Young H. Yuh, and Jenn Huei Lii. Molecular mechanics. the mm3 force field for hydrocarbons. 1. *J. Am. Chem. Soc.*, 111:8551–8566, 1989.

9. Norman L. Allinger, Fanbing Li, and Liqun Yan. Molecular mechanics. the mm3 force field for alkenes. *J. Comput. Chem.*, 11:848–867, 1990.
10. Norman L. Allinger, Xuefeng Zhou, and John Bergsma. Molecular mechanics parameters. *J. Mol. Struct. Theochem*, 312:69 – 83, 1994.
11. Jay W. Ponder and Frederic M. Richards. An efficient newton-like method for molecular mechanics energy minimization of large molecules. *J. Comput. Chem.*, 8:1016–1024, 1987.
12. H. J. C. Berendsen, J. P. M. Postma, W. F. van Gunsteren, A. DiNola, and J. R. Haak. Molecular dynamics with coupling to an external bath. *J. Chem. Phys.*, 81:3684–3690, 1984.
13. Shuai, Zhigang, Wang, Linjun, and Song, Chenchen. *Theory of Charge Transport in Carbon Electronic Materials*. Springer, 2012.
14. J Cornil, S Verlaak, N Martinelli, A Mityashin, Y Olivier, T Van Regemorter, G D’Avino, L Muccioli, C Zannoni, F Castet, D Beljonne, and P Heremans. Exploring the Energy Landscape of the Charge Transport Levels in Organic Semiconductors at the Molecular Scale. *Acc. Chem. Res.*, 2012.
15. Lin, Lili, Geng, Hua, Shuai, Zhigang, and Luo, Yi. Theoretical insights into the charge transport in perylene diimides based n-type organic semiconductors. *Neutron Spin Echo In Polymer Systems*, 13:2763–2772, 2012.
16. Tahsin J Chow. *Organic Structures Design. Applications in Optical and Electronic Devices*. CRC Press, 2014.
17. M. Sato, A. Kumada, K. Hidaka, T. Hirano, and F. Sato. Computational study on electron mobility in liquid benzene. In *2016 IEEE International Conference on Dielectrics (ICD)*, volume 2, pages 844–847, 2016.
18. Yihan Shao, Zhengting Gan, Evgeny Epifanovsky, Andrew T.B. Gilbert, Michael Wormit, Joerg Kussmann, Adrian W. Lange, Andrew Behn, Jia Deng, Xintian Feng, Debashree Ghosh, Matthew Goldey, Paul R. Horn, Leif D. Jacobson, Ilya Kaliman, Rustam Z. Khaliullin, Tomasz Kus, Arie Landau, Jie Liu, Emil I. Proynov, Young Min Rhee, Ryan M. Richard, Mary A. Rohrdanz, Ryan P. Steele, Eric J. Sundstrom, H. Lee Woodcock III, Paul M. Zimmerman, Dmitry Zuev, Ben Albrecht, Ethan Alguire, Brian Austin, Gregory J. O. Beran, Yves A. Bernard, Eric Berquist, Kai Brandhorst, Ksenia B. Bravaya, Shawn T. Brown, David Casanova, Chun-Min Chang, Yunqing Chen, Siu Hung Chien, Kristina D. Closser, Deborah L. Crittenden, Michael Diedenhofen, Robert A. DiStasio Jr., Hainam Do, Anthony D. Dutoi, Richard G. Edgar, Shervin Fatehi, Laszlo Fusti-Molnar, An Ghysels, Anna Golubeva-Zadorozhnaya, Joseph Gomes, Magnus W.D. Hanson-Heine, Philipp H.P. Harbach, Andreas W. Hauser, Edward G. Hohenstein, Zachary C. Holden, Thomas-C. Jagau, Hyunjun Ji, Benjamin Kaduk, Kirill Khistyayev, Jaehoon Kim, Jihan Kim, Rollin A. King, Phil Klunzinger, Dmytro Kosenkov, Tim Kowalczyk, Caroline M. Krauter, Ka Un Lao, AdÁšle D. Laurent, Keith V. Lawler, Sergey V. Levchenko, Ching Yeh Lin, Fenglai Liu, Ester Livshits, Rohini C. Lochan, Arne Luenser, Prashant Manohar, Samuel F. Manzer, Shan-Ping Mao, Narbe Mardirossian, Aleksandr V. Marenich, Simon A. Maurer, Nicholas J. Mayhall, Eric Neuscammann, C. Melania Oana, Roberto Olivares-Amaya, Darragh P. O’Neill, John A. Parkhill, Trilisa M. Perrine, Roberto Peverati, Alexander Prociuk, Dirk R. Rehn, Edina Rosta, Nicholas J. Russ, Shaama M. Sharada, Sandeep Sharma, David W. Small, Alexander Sodt, Tamar Stein, David StÁeck, Yu-Chuan Su, Alex J.W. Thom, Takashi Tsuchimochi, Vitalii Vanovschi, Leslie Vogt, Oleg Vydrov, Tao Wang, Mark A. Watson, Jan Wenzel, Alec White, Christopher F. Williams, Jun Yang, Sina Yeganeh, Shane R. Yost, Zhi-Qiang You, Igor Ying Zhang, Xing Zhang, Yan Zhao, Bernard R. Brooks, Garnet K.L. Chan, Daniel M. Chipman, Christopher J. Cramer, William A. Goddard III, Mark S. Gordon, Warren J. Hehre, Andreas Klamt, Henry F. Schaefer III, Michael W. Schmidt, C. David Sherrill, Donald G. Truhlar, Arieh Warshel, Xin Xu, AlÁjn Aspuru-Guzik, Roi Baer, Alexis T. Bell, Nicholas A. Besley, Jeng-Da Chai, Andreas Dreuw, Barry D. Dunietz, Thomas R. Furlani, Steven R. Gwaltney, Chao-Ping Hsu, Yousung Jung, Jing Kong, Daniel S. Lambrecht, WanZhen Liang, Christian Ochsenfeld, Vitaly A. Rassolov, Lyudmila V. Slipchenko, Joseph E. Subotnik, Troy Van Voorhis, John M. Herbert, Anna I. Krylov, Peter M.W. Gill, and Martin Head-Gordon. Advances in molecular quantum chemistry contained in the q-chem 4 program package. *Mol. Phys.*, 113:184–215, 2015.
19. Chao-Ping Hsu. The Electronic Couplings in Electron Transfer and Excitation Energy Transfer. *Acc. Chem. Res.*, 42:509–518, 2009.
20. KA Fichthorn and WH Weinberg. Theoretical foundations of dynamic monte-carlo simulations. *J. Chem. Phys.*, 95:1090–1096, 1991.

21. Lingyi Meng, Yuan Shang, Qikai Li, Yongfang Li, Xiaowei Zhan, Zhigang Shuai, Robin G E Kimber, and Alison B Walker. Dynamic Monte Carlo Simulation for Highly Efficient Polymer Blend Photovoltaics. *J. Phys. Chem. B*, 114:36–41, 2010.